Supplementary material for: Resuspension of droplets

Mehdi Maleki, Clément de Loubens,* and Hugues Bodiguel
Univ. Grenoble Alpes, CNRS, Grenoble INP, LRP, 38000 Grenoble, France
(Dated: October 13, 2021)

CONTENTS

I. DROPLET PRODUCTION

The oil-in-water emulsions were produced with two different methods: microfluidics and membrane emulsification. Monodisperse emulsions were fabricated by microfluidics method while polydisperse emulsions were produced by membrane emulsification. The aqueous phase consisted of water-glycerol mixture (glycerol 84 % w/w, CAS number 56-81-5, VWR) and added food grade colorant (0.001% w/w, E122, Breton). The oil phase was composed of medium chain triglyceride oil (Nestlé, Switzerland) with sorbitan trioleate 85 (1% w/w, CAS number 26266-58-0, Sigma-Aldrich). Table I shows the physical properties of oil and water phases of the emulsions.

TABLE I. Physical properties of oil and water phases of the emulsions at 23 °C.

Phase	Density $kg.m^{-3}$	Viscosity mPa.s	Refractive Index nD
Oil Phase	943.42	50	1.44948
Water Phase	1218.52	85	1.44948

* clement.de-loubens@univ-grenoble-alpes.fr

Monodisperse oil-in-water emulsions were produced with a custom-made PMMA T-junction microfluidic chip with a cross-section 1×1 mm. The inside of the chip was treated with acetone in order to render the surface hydrophilic. As shown in figure 1-right, the continuous aqueous phase was injected through the main channel while the dispersed oil phase was introduced through the perpendicular branch via a round glass capillary (CM Scientific Ltd) of 300 μm inner diameter. The flow rates were controlled by two syringe pumps (neMSYS, CETONI). To improve the production rate, T-junction chip was modified by narrowing the intersection area to strength shear forces. Two monodisperse emulsions with different droplet sizes were generated at volumetric frow rates of oil phase 0.2 and 0.3 mL/min while the flow rate of aqueous phase 2 mL /min in both cases.

The lab-scale membrane emulsification system was purchased from Micropore Technologies Ltd (UK) under the commercial name Micropore LDC-1. The system includes a micro-engineered emulsification membrane with 20 μm cylindrical laser etched pores under a paddle-blade stirrer (Figure 1-left). The rotational velocity of the stirrer was controlled by a DC motor. The thin flat nickel emulsification membrane was chemically treated on one side to have a hydrophilic surface. The pore spacing and porosity of the membrane were 200 μm and 0.91% respectively. The array of pores was located in an narrow annular region on the membrane to limit the variation of shear rate and thus homogenize the droplet size distribution [1]. The aqueous phase was stirred with the paddle at 500 rpm and the oil phase was injected by a syringe pump (neMSYS, CETONI) through the membrane with a flow rate of 2 ml/min.

II. SIZE DISTRIBUTION

The estimation of the droplet size distribution was based on bright field microscopy images. A large amount of droplets was placed on wide microscope slides and put under an inverted microscope (IX-73, Olympus) equipped with 4, 10, and 20 fold objectives. The motorized stage (Marzhauser) was automatized to perform a tile scan on the entire specimen and the pictures were acquired with a digital camera (ORCA-Flash 4.0, Hamamatsu). The droplet size was measured with a custom written software based on the Matlab (The MathWorks, Inc.) image processing toolbox. The average radius of the monodisperse droplets were $a = 143$ and $185\,\mu$m and polydisperse droplets $a = 47\,\mu$m with a sampling

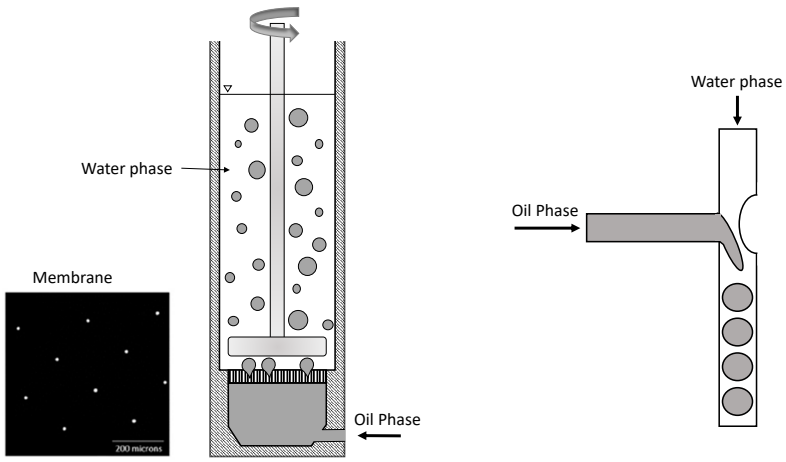

FIG. 1. Production of droplet emulsions. **Left:** Membrane emulsification system to produce poly dispersed droplets, **Right:** Microfluidic T-junction chip to produce monodispesed droplets

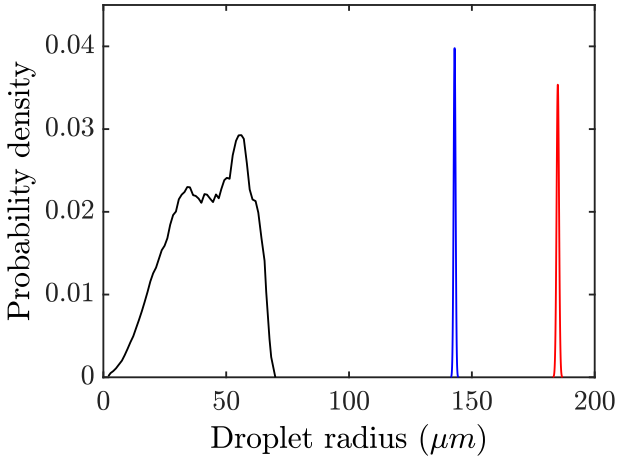

FIG. 2. Probability density of volumic size distribution of droplets. Polydisperse emulsion was resulted from membrane emulsification system and monodisperse emulsion was produced by microfluidic system.

rate over several thousand. The size distribution of the monodisperse and polydisperse emulsions is shown in Figure 2.

III. PARALLAX ISSUE

In this section, we analyze the parallax issue raised by the finite distance between the camera and Taylor-Couette geometry. In the experimental setup, the light source was a 2D LED panel with a homogeneous and stable light intensity. It was placed parallel to the Taylor-Couette geometry with 10 cm of distance. As shown in figure 3-right, light beams traveled through the suspension and geometry, then they were collected by a camera (Basler, acA2500-14gc), located at a distance of L from the geometry.

By considering a finite value of L, the camera received the incident light beams within an angle of 0 to α relative to the horizontal direction. This lead to a smoothing effect on the concentration profile in the vertical direction x_3 through a length of l (figure 3-right). This means that the measurement of the droplet concentration was vertically averaged in this length. Consequently, the errors induced by smoothing could be considerable where the vertical concentration sharply shifted to zero at the nose of the suspension as shown in figure 7. Note that, measuring of normal viscosity $\eta_{n,3}$ and determining exponent n in SBM model depends strongly on the precision to detect the curvature of the concentration transition to zero.

By increasing the distance L between the camera and the geometry, the angle α and the vertical averaging length l reduced. Consequently, the spatial smoothing of the concentration profile in the vertical direction became less effective. The experiments were performed with a distance of L up to 5 m, whereas the height of the suspension in the measurement zone was 2 cm. To have high resolution images (5 pixels for a droplet diameter) we used a lens with a large focal length. Figure 3-left represents an image of the geometry with two similar rulers placed at two sides of the geometry. We can observe that the parallax in the measurement zone was negligible. However it became more decisive near the bottom of the geometry. In such configuration of the experimental setup, we estimated $\alpha = 0.11$ degree and vertical averaging length $l = 96\,\mu$m. The ratio of l to the diameter of monodisperse and polydisperse droplets is $l/a = 1/3$ and 1 respectively. These small ratios indicated a neg-

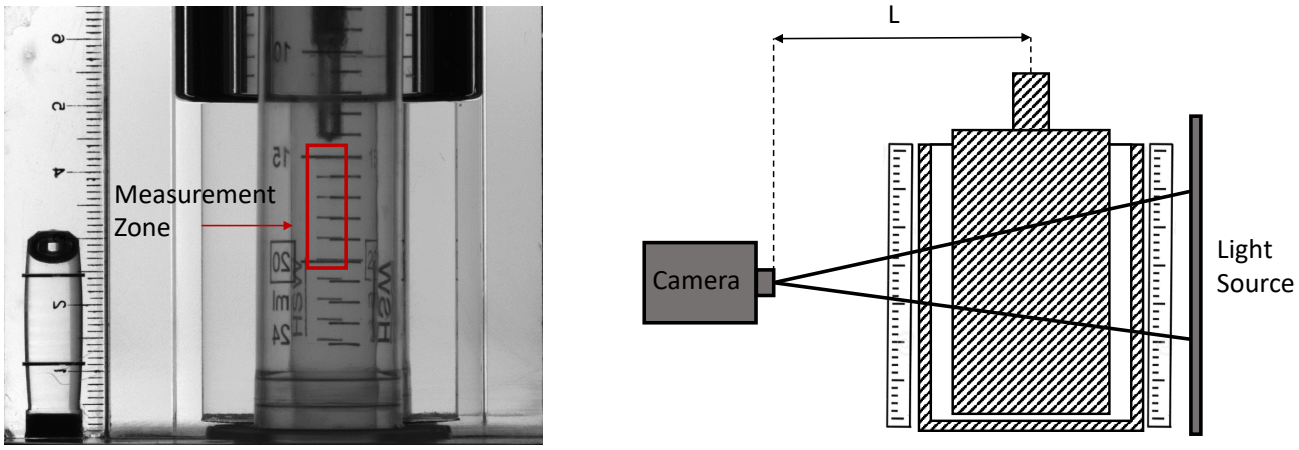

FIG. 3. Parallax issue along the vertical direction solved by increasing the distance L between the camera and Taylor-Couette cell up to five meters. To have high resolution pictures of measurement zone a lens with a large focal length has been used. A ruler behind and front of the Taylor-Couette cell indicates a negligible parallax issue.

ligible effect of the parallax on the concentration profile measurement where it experienced a sharp transition to zero. Consequently, the parallax did not impact the comparison of our measurements with SBM model.

IV. TUNING REFRACTIVE INDEX

Balancing the refractive index between the droplets and suspending fluid was crucial for our experimental method. Light refraction between the two phases in the emulsions could give rise to considerable errors in the measurement of the concentration profile $\phi(x_3)$. The refractive index of the oil phase was measured with precise refractometer (Abbemat 350, Anton Paar) $n = 1.44948$ nD at $T = 23$ °C and wavelength $\lambda = 589$ nm. Note that the resuspension experiments were conducted at the same temperature and a wavelength band of $\lambda = 525 \pm 15$ nm. Figure 4 illustrates the difference of refractive index between the droplets and suspending fluid for various glycerol volume fractions in the suspending fluid. The zero contrast was estimated with a glycerol volume fraction around $\phi = 84.68\%$ w/w. Then after preparing the solution, the contrast was refined to a precision of $\Delta n = 0.00000$ nD with drop-by-drop addition of glycerol or water and mixed. After that 1 mL of the solution was pipetted from different cites in the solution volume. The refractive index of these samples was measured to the precision $\Delta n = 0.00000$ nD and in the case of mismatch the process was repeated.

V. CHARACTERIZING THE ABSORBANCE

The vertical concentration profile of the resuspended emulsions $\phi(x_3)$ was obtained by the light absorption

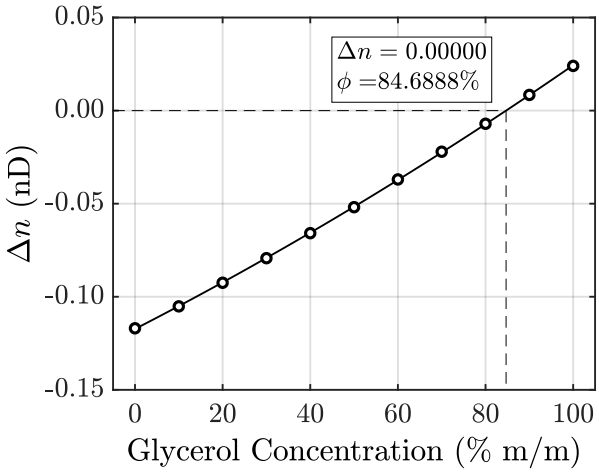

FIG. 4. The difference of refractive index between the droplets and suspending fluid as a function of glycerol volume fraction at 23 °C and wavelength $\lambda = 589$ nm. A zero contrast of refractive index was estimated with glycerol concentration $\phi = 84.6888\%$. The final contrast was refined to a precision of $\Delta n = 0.00000$ nD by adding some drops of glycerol or water.

technique. Since the droplets and suspending fluid were both completely transparent, adding a colorant to the suspending fluid provided a contrast in the light absorbance degree between the two phases. A non-fluorescent food-grade additive, E122 (Breton) was used as the colorant. UV-Vis spectrophotometry analysis of the colorant was performed in a quartz cuvette (Hellma Analytics) with a light path of $L = 2$ mm and a portable spectrometer (RedLite, Ocean Insight). Figure 5-left demonstrates the absorption spectra of the colorant dissolved in the suspending fluid with the concentration ranging from $c = 0.001\%$ to 0.04% mg/ml. The ab-

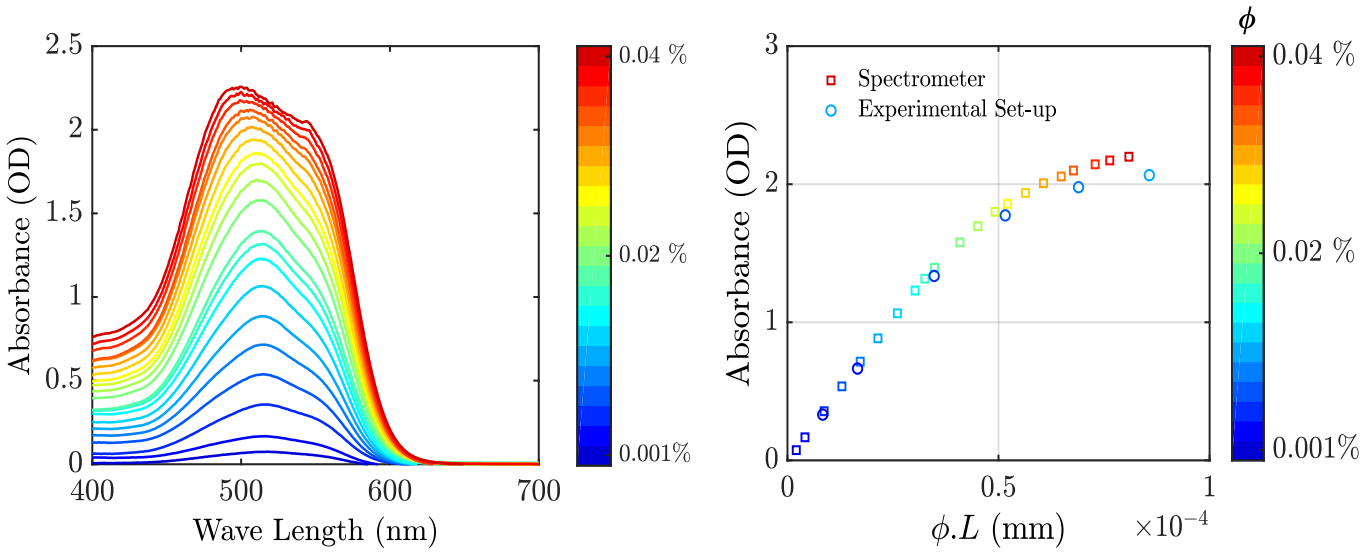

FIG. 5. Characterization of the light absorbance of the colorant, **Left:** The light absorbance of the colorant for concentration ranging from $c = 0.001\%$ to 0.04% mg/mL in visible light wave length measured by a spectrometer in a $L = 2$ mm cuvette, **Right:** Absorbance of the colorant at wave length $\lambda = 525$ nm as a function of ϕL, where ϕ is the colorant concentration and L is the traveled length of light in the sample. The measured absorbance by the spectrometer in a cuvette with $L = 2$ mm has an excellent agreement in the linear part with measured absorbance by the experimental set-up in the Taylor-Couette cell. A bandpass filter with the center wavelength, $\lambda = 525 \pm 15$nm was used in the experimental set-up.

sorption spectrum was a broad band with a maximum absorbance peak at $\lambda = 520$ nm.

To validate our experimental approach, we measured the absorbance of the colorant with a digital camera (acA2500-14gc, Basler) in Taylor-Couette Cell and compared the results with a spectrophotometer. As shown in figure 5-left, the wavelength related to the peak of absorbance was around $\lambda = 520$ nm, thus we used an interference bandpass filter with the center wavelength $\lambda = 525 \pm 15$ nm. Beer-Lambert law formulates the exponential decay of the light intensity passing through a solution. Thus we related intensities and a distance L and calculated the absorbance as:

$$A \equiv log(\frac{I_0 - I_d}{I_L - I_d}) = \varepsilon c L \tag{1}$$

where I_0 is the light intensity after traveling the suspending fluid without colorant as well as the transparent container cell of sample, I_L is the traveled light intensity with contribution of the colorant, I_d is the measured light intensity by the insulated camera which represents the noise and ε is the attenuation rate of light for the colorant. Contrary to the cuvette, in Taylor-Couette cell, the traveled length of the light beam through the sample was not constant. By determining the corresponding traveled length L for each pixel of the captured image, a 2D light absorbance map was obtained. As expected, for the homogeneous colorant solution in Taylor-Couette cell, we obtained an uniform 2D absorbance map. Figure 5-right demonstrates the absorbance of the colorant at wavelength $\lambda = 520$ nm, measured by the spectrophotometer and the experimental setup as a function of $\phi.L$ where ϕ is the colorant concentration and L is the traveled length of light in the sample. The measurements show an excellent consistency in the linear regime. The experiments were conducted in such fashion to keep the corresponding absorbance values within the linear part.

VI. COALESCENCE ISSUE

As the droplets were less dense than the suspending fluid, they creamed on top of the Taylor-Couette cell. The droplets could be deformed under the buoyant force, which causes them to coalesce [2]. The droplet coalescence was inhibited with a surface treatment of the geometry for monodisperse suspensions. However, this surface treatment proved to be inefficient for polydisperse suspensions. Figure 6-a shows the concentration map of the polydisperse droplets in $x_1 - x_3$ plane for shear rates ranging from $\dot{\gamma} = 0$ to 87 s^{-1} in steady state. It illustrates the emergence and then stabilization of the oil layer caused by coalescence at the top of the geometry. Additionally, we observed that the creamed suspension underwent a similar transformation over a short period of time even at rest. However, under a shear stress, this process slowed down. We had to make a correction in the experimental data in order to discard the coalesced part and took into account only the true quantity of droplets in the suspension. This was necessary since the migration phenomenon in the resuspension experiments depended on the droplet quantity. Moreover, comparing the migration rate in the same suspension as a function of shear rate was possible only if the non-coalesced droplet quan-

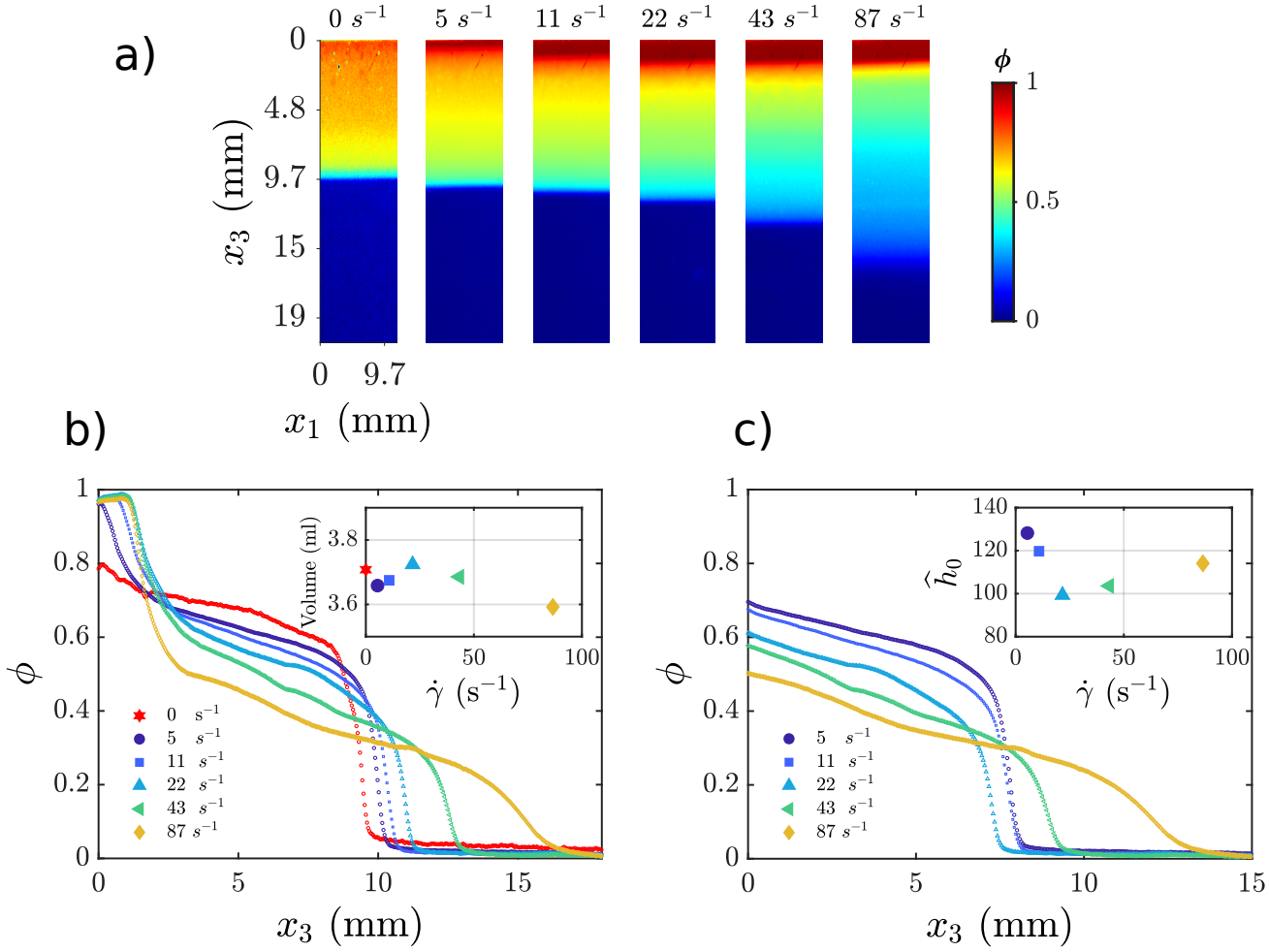

FIG. 6. Coalescence issue for polydisperse suspensions despite surface treatment, **a:** 2D concentration profile of droplets in $x_1 - x_3$ plane and presence of an oil layer at the top of the Taylor-Couette cell resulted from coalescence of droplets, **b:** The concentration profile of droplets in steady state along the resuspension direction x_3 for shear rates ranging from $\dot{\gamma} = 0$ to 87 s^{-1}. The coalesced part was detected by sharp increase of the concentration. Insert figure is the total volume of oil phase calculated by equation 2. **c:** Corrected concentration profile of droplets as a function of x_3. Inset figure is normalized height of the creamed suspension at rest $\widehat{h}_0 = h/a$ calculated by the equation 3 as a function of shear rate. h is the height of resuspension in the steady state and a is the average size of the droplets.

tity was taken into account.

Figure 6-b shows the vertical steady state concentration profile of droplets $\phi(x_3)$ for shear rates ranging from $\dot{\gamma} = 0$ to 87 s^{-1} . The total volume of the oil phase (droplets and coalesced part) was calculated by integrating $\phi(x_3)$ over x_3:

$$V = \pi(R_2^2 - R_1^2) \int_0^H \phi(x_3)\, dx_3 \qquad (2)$$

where $R_1 = 20$, $R_2 = 24$ and $H = 50$ mm are the inner, outer radii and height of the Taylor-Couette cell respectively. The total volume of oil phase (inset figure 6-b) was V= 3.691 $\pm$ 0.033 ml for shear rates up to $\dot{\gamma} = 43$ s^{-1} which corresponds to a relative standard deviation from 2.7 % up to = 5.2 % at $\dot{\gamma} = 87$ s^{-1}. This variation increment originated from the optical issues at the surface of oil layer with the air. The coalesced part was detected by a sharp increase in the concentration profile near $x_3 = 0$. Figure 6-c shows the same concentration profiles after eliminating the part related to the coalescence. Consequently, each concentration profile was a representation of the droplets migration as a response to the shear rate but with different quantities of particles in the suspension. Based on the mass conservation, by integrating the concentration profile over the normalized length $\widehat{x}_3 = x_3/a$, we estimated the normalized height of the creamed suspension at rest $\widehat{h}_0$ for each concentration profile:

$$\widehat{h}_0 \phi_m = \int_0^{\widehat{h}} \phi(\widehat{x}_3)\, d\widehat{x}_3 \qquad (3)$$

where $\widehat{h}$ is the normalized height of the suspension in steady state, and took $\phi_m = 0.76$. The inset of figure

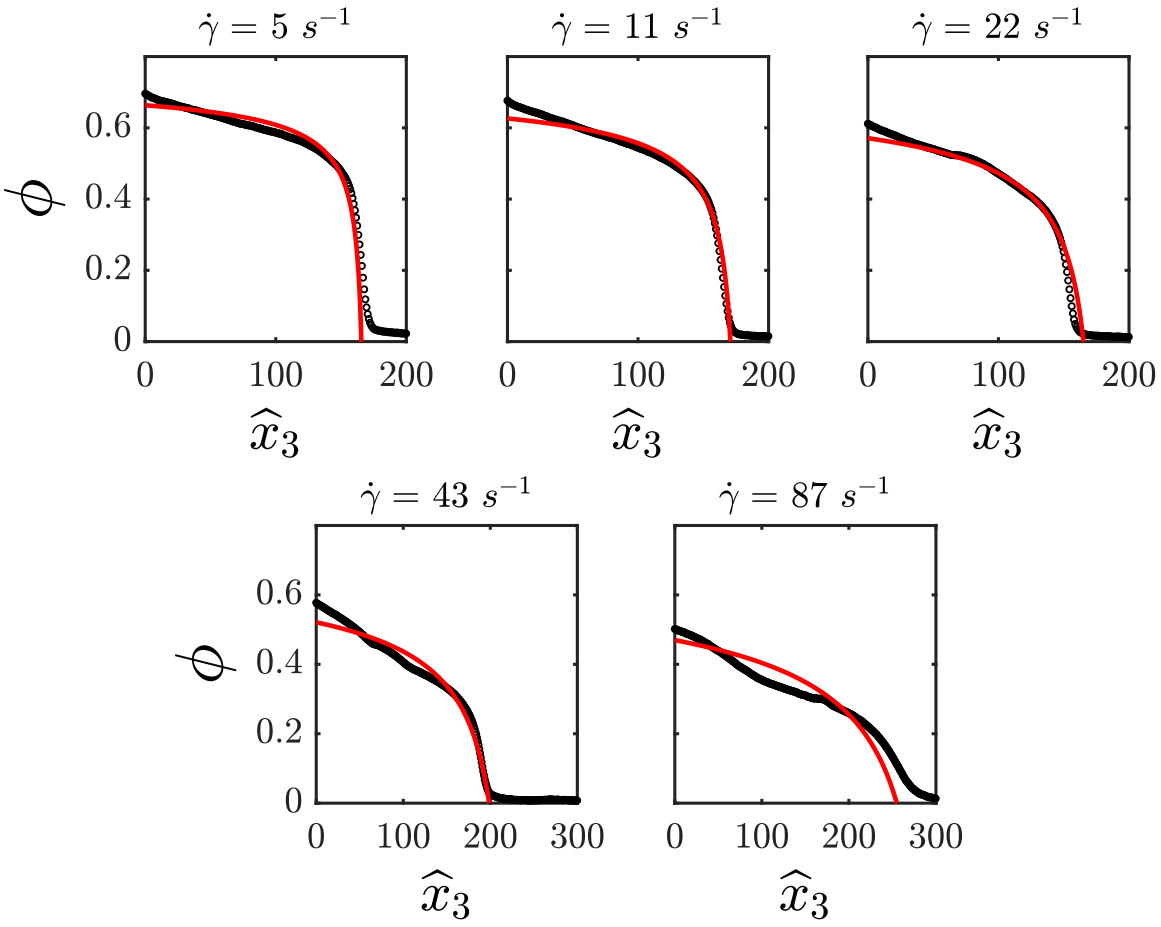

FIG. 7. Corrected concentration profile of polydisperse suspension of droplets for shear rates in the range of $\dot{\gamma} = 5$ to 87 s^{-1}. The circles are the experimental data from section VI and solid lines are the analytical profiles based on the Suspension Balance Model with $n = 2$ and calculated from equation 4 with $\phi_m = 0.76$ and $\lambda_3 = 0.69$.

6-c shows the calculated $\widehat{h}_0$ for each concentration profile which is in the range of 100 to 128 . The increase of $\widehat{h}_0$ for shear rates $\dot{\gamma} = 43$ and 87 s^{-1} can be attributed to the break-up of the large oil pockets which did not coalesce with the oil layer located at the top of the geometry. To compare our results, such as the normal viscosity $\eta_{n,3}$, the evolution of suspension height $\widehat{h}$ and concentration profile $\phi(\widehat{x}_3)$, to Suspension Balance Model (SBM) we used the corrected data.

VII. CONCENTRATION PROFILES AT REST

At rest and after creaming during about 12h, the volume fraction was not uniform but exhibited a gradient from about 0.6 at the bottom of the emulsion layer up to 0.8 at the top. This effect was the signature of droplet deformability, since - at least for monodisperse systems - a volume fraction of 0.8 cannot be obtained with spherical droplets. je ne comprend pas la phrase suivante When comparing the particle stress, given by $\Sigma_{p,33} = \int \Delta\rho g \phi dx_3$ with the Laplace pressure, we indeed found that the particle stress was a non negligible fraction of Laplace pressure, which allowed significant deformation of the droplet.

In Fig. 8, the volume fraction at rest is plotted for the three systems studied as a function of the Laplace number, $La = \Sigma_{p,33}/(\gamma/a)$. The two monodisperse systems nicely collapsed on a master curve, which was roughly an affine function of La. This validated the above hypothesis that the droplet deform due to the buoyant mass of the layer underneath. The polydisperse system slighlty deviated from this behaviour in the bottom of the layer, which might indicate that a size segregation existed in this case.

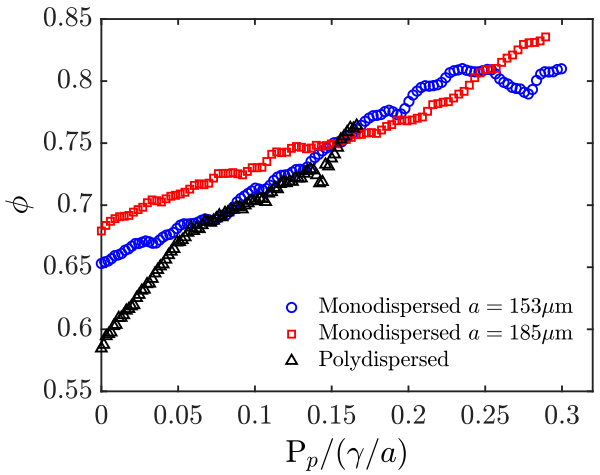

FIG. 8. Concentration profiles at rest ($\dot{\gamma} = 0$) as a function of the Laplace number L_A for monodispersed and polydispersed suspenions of droplets.

VIII. CONCENTRATION PROFILE OF POLYDISPERSE SUSPENSION

Based on the theoretical framework of the Suspension Balance Model (SBM), in the case of $n = 2$, the concentration profile of the droplets was calculated analytically as [3]:

$$\frac{\phi(\widehat{x}_3)}{\phi_m} = 1 - \left[1 + \frac{\phi_m}{\lambda_3 Sh}(\widehat{h} - \widehat{x}_3)\right]^{-1/2} \tag{4}$$

where the normalized steady state height of the suspension $\widehat{h}$ is

$$\widehat{h} = \widehat{h}_0 + 2\sqrt{\frac{\lambda_3 \widehat{h}_0}{\phi_m} Sh} \tag{5}$$

Figure 7 represents the corrected concentration profiles of the polydisperse suspension and the analytical profile calculated by equation 4 for shear rates ranging from $\dot{\gamma} = 5$ to 87 s^{-1}. Jamming concentration was $\phi_m = 0.76$ and the best fit was found with free parameter $\lambda_3 = 0.69$. The experimental results for shear rates $\dot{\gamma} = 5$ to 43 s^{-1} were in good agreement with the theoretical prediction in equation 4. In the case of $\dot{\gamma} = 87$ s^{-1} the inertia effects came into play. Furthermore, the discrepancies between the experimental and theoretical results could originated from the structuration of the droplets caused by size polydispersity.

IX. SUSPENSION HEIGHT EVOLUTION

Normalized height of the suspensions for shear rates in the range of $\dot{\gamma} = 5$ to $135 s^{-1}$ is presented in figure 9 as a function of Acrivos number. Acrivos number is defined:

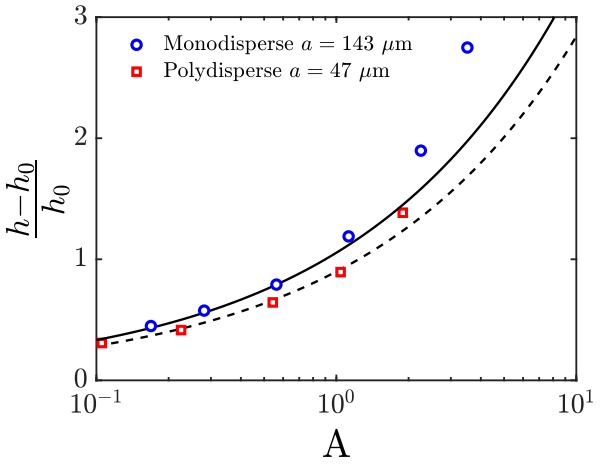

FIG. 9. Variation of the normalize height of resuspended monodisperse and polydisperse suspensions as a function of Acrivos number. Solid line is the correlation with $n = 2$, $\phi_m = 0.8$ and $\lambda_3 = 1$ for monodisperse droplets and dashed line with $n = 2$, $\phi_m = 0.76$ and $\lambda_3 = 0.69$ for monodisperse and polydisperse droplets respectively.

$$A = \frac{\eta_0 \dot{\gamma}}{\Delta \rho g h_0} \tag{6}$$

which is the ratio of viscous force to buoyancy force as Shields number Sh but with h_0 for the characteristic length. The analytical correlation presented in equation 5 is traced for monodisperse droplets (solid line) with $n = 2$, $\phi_m = 0.8$ and $\lambda_3 = 1$ and for polydisperse droplets (dashed line) with $n = 2$, $\phi_m = 0.76$ and $\lambda_3 = 0.69$. We observed that the experimental results for both monodisperse and polydisperse suspensions were in excellent agreement with the theoretical correlation in the range of $0.1 < A < 1$. In contrast, a divergence was found for higher values of A which can be due to the inertial effects.

[1] S. R. Kosvintsev, G. Gasparini, R. G. Holdich, I. W. Cumming, and M. T. Stillwell, Industrial & engineering chemistry research **44**, 9323 (2005).
[2] M. Henschke, L. H. Schlieper, and A. Pfennig, Chemical Engineering Journal **85**, 369 (2002).
[3] B. Saint-Michel, S. Manneville, S. Meeker, G. Ovarlez, and H. Bodiguel, Physics of Fluids **31**, 103301 (2019).